

Nanoscale

Accepted Manuscript



This is an *Accepted Manuscript*, which has been through the Royal Society of Chemistry peer review process and has been accepted for publication.

Accepted Manuscripts are published online shortly after acceptance, before technical editing, formatting and proof reading. Using this free service, authors can make their results available to the community, in citable form, before we publish the edited article. We will replace this *Accepted Manuscript* with the edited and formatted *Advance Article* as soon as it is available.

You can find more information about *Accepted Manuscripts* in the [Information for Authors](#).

Please note that technical editing may introduce minor changes to the text and/or graphics, which may alter content. The journal's standard [Terms & Conditions](#) and the [Ethical guidelines](#) still apply. In no event shall the Royal Society of Chemistry be held responsible for any errors or omissions in this *Accepted Manuscript* or any consequences arising from the use of any information it contains.

Peculiar pressure effect on Poisson ratio of graphone as a strain damper[†]

Qing Peng,^{1*} Albert K. Dearden,² Xiao-Jia Chen,³ Chen Huang,² Xiaodong Wen,^{4,5} and Suvarnu De¹

Received Xth XXXXXXXXXXXX 20XX, Accepted Xth XXXXXXXXXXXX 20XX

First published on the web Xth XXXXXXXXXXXX 200X

DOI: 10.1039/b000000x

Hydrogenation is an effective way to modify the electronic and magnetic properties of graphene. The semi-hydrogenated graphene, known as “graphone”, has promising applications in nanoelectronics including field-effect transistors. However, the elastic limit of this two-dimensional material remains unknown despite its importance in applications as well as strain engineering to tailor functions and properties. Here we report using first-principles calculations an abnormal increase in the Poisson ratio of graphone in response to an increase in pressure. This peculiar behavior is proposed to originate from the asymmetry of hydrogenation and could be used to design a nanodevice of strain damper to reduce harmful strains in graphene-based nanoelectronics.

Graphone is a derivative of graphene with only one side fully hydrogenated^{1–7}. It is experimentally fabricated by removing the hydrogen on one side from graphane^{8–10}, the fully hydrogenated graphene that has hydrogen on both sides¹¹. If we score the performance of hydrogenation, graphene, graphone, and graphane are 0, 50, and 100 respectively. By 50% hydrogenation, graphone possesses a small indirect bandgap, which is quite different from both graphene (zero bandgap) and graphane (large direct bandgap), implying potential applications in field-effect transistors¹², logic devices, and high-speed switching devices¹³, in addition to hydrogen-storage. More importantly, graphone exhibits magnetism and is able to

react with electronic and magnetic fields, which is crucially important for applications in nanoelectronics and spintronics¹⁴. The magnetic moments from unpaired electrons on the unhydrogenated carbon atoms are ferromagnetically coupled, resulting in an infinite magnetic sheet that has homogeneous magnetism in addition to structural integrity in a single layer¹. Compared to other methods of engineering magnetism, hydrogenation of graphene to graphone is a relatively easy way to obtain magnetism in graphene based nanoelectronics. Furthermore, graphone is thermodynamically stable¹⁵, which avoids the difficulty of obtaining a magnetic structure through cutting of graphene sheets and thus provides a unique structure for the use of magnetism in nanomaterials. In forming graphone by hydrogenation of graphene on the substrate of hexagonal boron nitride, two great challenging problems (finite band gaps and suitable substrates) are resolved at the same time¹⁶, holding great promise for advanced post-silicon electronics¹⁷.

A graphone monolayer could be free-standing, on a substrate, or sandwiched by other layers in real applications. In these cases, it will be strained for two factors as atomic thickness and the presence of strain fields in the environment: for instance, lattice mismatch, surface corrugation of substrates, and spontaneous elastic waves due to vibrations. The strains could profoundly change the properties of graphone monolayers including band structures, magnetism, strengths, and instabilities¹⁸. Therefore, knowing the elastic properties, including elastic limits and high order elastic constants, is critical in design and practical applications¹⁹. Particularly, the elastic limit sets the upper boundary of the mechanical load²⁰ and high order elastic constants describe the non-linear elastic behaviors before material failure. However, it is a great challenge to measure the elastic limits of the graphone monolayers experimentally in addition to its synthesis and manipulation due to the extremely small thickness. To the authors' best knowledge, there is no experimental report of the structure parameters and elastic properties of graphone. Alternatively, theoretical predictions are also a nontrivial task due to both debonding under extreme loadings and the linkage between atomistic modeling and continuum elastic theory. Here, we report a sys-

[†] Electronic Supplementary Information (ESI) available: The atomic structural parameters, ultimate stresses and strains, and elastic constants (up to fifth order) are summarized. The calculations use three other exchange-correlation functionals. See DOI: 10.1039/b000000x/

¹Department of Mechanical, Aerospace and Nuclear Engineering, Rensselaer Polytechnic Institute, Troy, NY 12180, U.S.A.

²Department of Scientific Computing, Florida State University, Tallahassee, FL, 32306, U.S.A.

³Center for High Pressure Science and Technology Advanced Research, Shanghai 201203, China.

⁴State Key Laboratory of Coal Conversion, Institute of Coal Chemistry, Chinese Academy of Sciences, Taiyuan, China, 030001

⁵Synfuels China Co. Ltd. Huairou, Beijing, China, 101407

*E-mail: qpeng.org@gmail.com

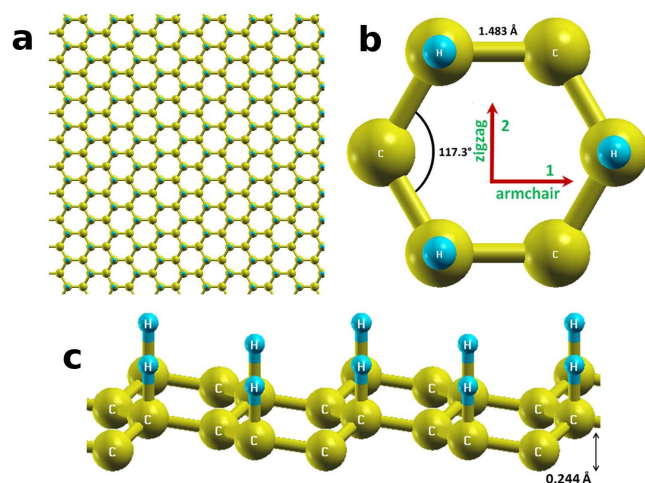


Fig. 1 Configurations of graphone. **a** graphone plane; **b** top-view and directions; **c** side-view.

tematic study on the elastic limits of graphone under mechanical strains using *ab initio* calculations. We find that graphone has a small in-plane stiffness (74%) as well as Poisson ratio (67%) compared to graphene, but similar to those of graphane. These results suggest that hydrogenation reduces the ultimate strength, ultimate strain, and Poisson ratio. In addition, the effect of hydrogenation on the mechanical properties is saturated when the graphene is only 50% hydrogenated.

We use a model of a unit cell consisted of three hydrogen and six carbon atoms, where a periodic boundary condition is applied only along x and y directions.

First-principles calculations in the frame of Density Functional Theory (DFT)²¹ are performed with the VASP code²², with the employment of projector augmented wave pseudo-potentials²³ where carbon's $2s^2 2p^2$ electrons and hydrogen's $1s^2$ electrons are treated as valence electrons. The exchange-correlation functionals are parameterized by Perdew, Burke, and Ernzerhof²⁴. We perform all the plane-wave DFT calculations with a kinetic-energy cutoff of 600 eV and a Gamma-centered $24 \times 24 \times 1$ k -mesh. After the structures are relaxed, the forces on each atom are smaller than 0.001 eV/Å. We set a vacuum region with a thickness of 20 Å in our model to reduce interactions between layers. However, such a vacuum region is user-defined, which may affect the Cauchy stresses calculated for the whole simulation box²². Therefore, the second Piola-Kirchhoff (P-K) stress is calculated to straighten out the ill-defined out-of-plane thickness of the monolayers²⁵. Lagrangian strain measures are used to capture the large deformation process. The three independent deformation models are necessary because they provide five stress-strain curves to compute the 14 independent components of elastic constants up to fifth order²⁵.

The stress-strain relationship is a unique characteristic of a material, like a “finger-print”. The elastic limits of this material can then be directly read from the stress-strain curves of tensile tests, where the maxima in stresses defines the ultimate stress. The corresponding strain to the ultimate stress is the ultimate strain. Graphone possesses a graphene-like honeycomb structure where there are two typical directions named “armchair” and “zigzag”, as depicted in Fig. 1 together with the geometry of its ground state (the structure parameters are in Table S1 in the Supporting Information). Strain uns from -0.1 to 0.4, with an increment of 0.01 for each of the three deformation modes examined in this work. Two of them are uniaxial deformations: one along the armchair direction and the other along the zigzag directions. The last is the biaxial deformation (equally deformed in both directions). The stress-strain relationships of graphone are shown in Fig. 2 compared with graphene and graphane²⁶. The strain limits of the armchair, zigzag, and biaxial deformations are 0.16, 0.21, and 0.22, respectively, and the stress limits are 19.8, 22.2, and 22.8 N/m respectively.

Graphone behaves asymmetrically in response to compressive (negative) and tensile (positive) strains. The systems under strains larger than the ultimate strains are unstable. They will not exist once perturbations are presented, including defects and thermodynamic motions²⁷. The ultimate strain measures the flexibility, which is correlated to the bond strengths. In addition, the ultimate strain is a lower limit of the critical strain, which provides a guide to strain-engineering as well as its various strain-related applications^{26,28}. The ultimate strengths as well as ultimate strains of the three deformation modes are summarized in Table S2 in the Supporting Information.

The elastic constants are the generalized “strength” of a material as derivatives of the stress-strain curves. Our results of the elastic constants from DFT calculations (Supporting Information Table S3) supply accurate parameters describing the elastic properties of graphone, which benefits the finite element modeling of graphone at the continuum level. The in-plane stiffness Y_s as well as Poisson's ratio ν are computed from the second order elastic constants C_{11} and C_{12} through the relationships of $Y_s = (C_{11}^2 - C_{12}^2)/C_{11}$ and $\nu = C_{12}/C_{11}$. The in-plane stiffness of Graphone's $Y_s = 251.7$ N/m is much smaller than that of graphene (340.8 N/m), which implies that the introduced hydrogen decreases the stiffness of graphene. The mechanism of such a reduction in stiffness could be due to the change in bonding characters caused by hydrogenation. For instance, the carbon-carbon bond in graphone (1.48 Å) is 4.4% longer than that in graphene which is 1.42 Å. Effectively, the carbon-carbon bonds in graphone are stretched and, as a result, weakened by hydrogenation. For the same reason, a similar reduction was also observed in graphane²⁶.

Besides the in-plane stiffness, the hydrogenation also re-

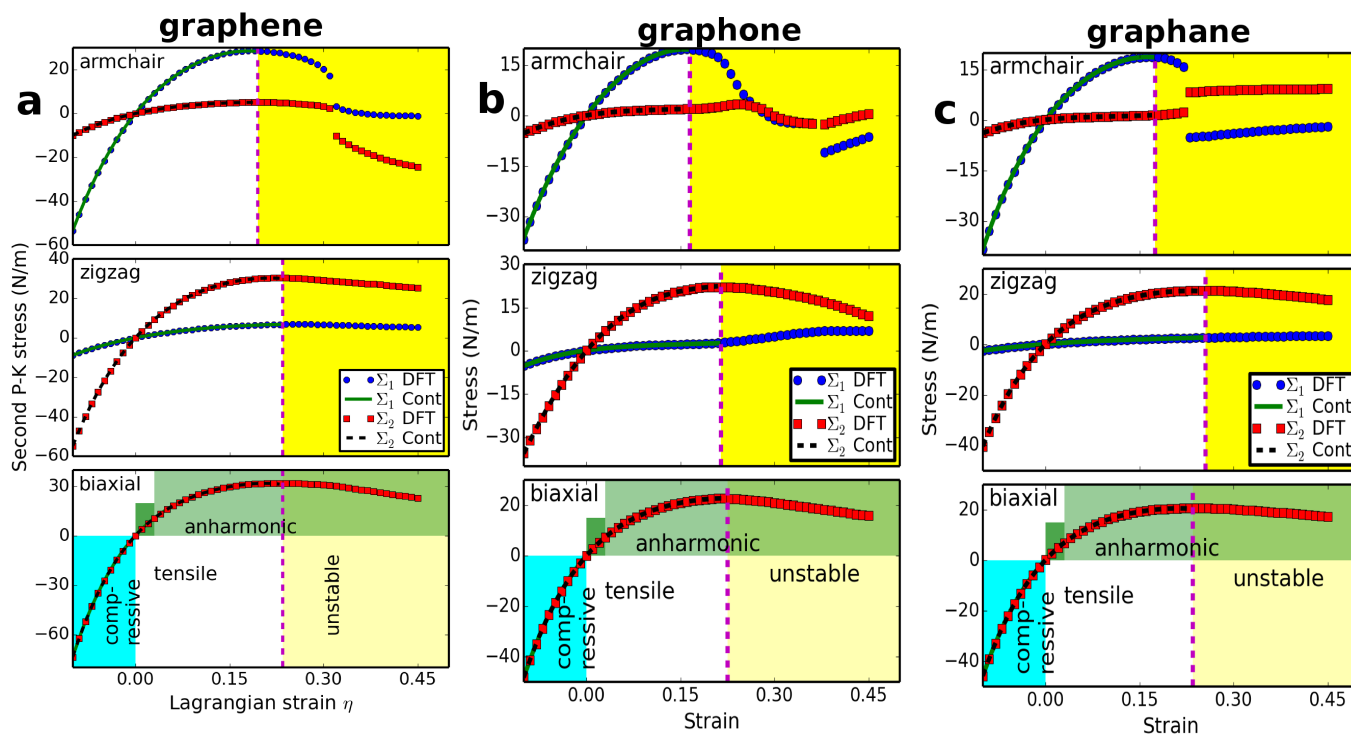


Fig. 2 Stress-strain responses. The second Piola-Kirchhoff stress²⁵ as a function of Lagrangian strain η for **a** graphene²⁶, **b** graphone, and **c** graphane²⁶ under the armchair (top), zigzag (middle), and biaxial (bottom) strains. Σ_1 (Σ_2) denotes the x (y) component of stress. “Cont” (lines for Σ_1 and dashed lines for Σ_2) stands for the fitting of DFT calculations (“DFT”, dots for Σ_1 and squares for Σ_2) to continuum elastic theory. The harmonic and anharmonic regions are within the elastic limit defined by ultimate strains. The systems under strains beyond the elastic limits are unstable. The strain limits of graphone are 0.16, 0.21, and 0.22 for armchair, zigzag, and biaxial deformations, respectively, with the stress limits of 19.8, 22.2, and 22.8 N/m respectively.

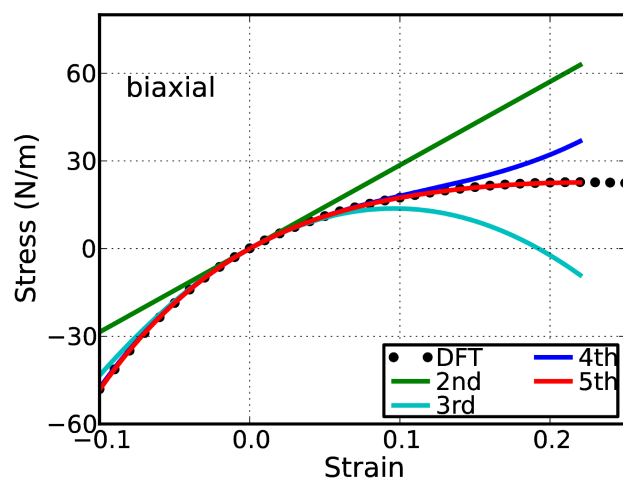


Fig. 3 Limits of higher order effects. Predicted stress-strain responses of biaxial deformation of graphone from different orders of elastic constants compared to that from the density functional theory (DFT) calculations (dotted line) indicates the limitations are 0.02, 0.07, 0.14, and 0.22 for second, third, fourth, and fifth order elastics, respectively.

duces the Poisson's ratio by a factor of 1/3 from graphene to graphone. The introduced hydrogen atoms form stiff carbon-hydrogen bonds which are perpendicular to the plane consisting of carbon atoms. These additional carbon-hydrogen bonds enhance the bending modes which involve the C-C-C angles, resulting in a low Poisson ratio. Such a reduction is also observed in other materials with stiff arms²⁹ including graphane²⁶. Compared to graphane, the elastic constants, bond lengths, in-plane stiffness, and Poisson ratio do not have many differences, as opposed to large differences between graphene and graphone, which indicates that the semi-hydrogenation of graphene already saturates the hydrogenation effect on mechanical strength.

Due to the extremely small thickness, the graphone monolayer is vulnerable to large strains where nonlinear elasticity is prominent. The high-order elastic constants are necessary to describe the nonlinear elastic behaviors, which for example, could be useful in strain-engineering nano-devices. Their importance could be demonstrated by their accuracy in modeling nonlinear elastic behaviors. Take the biaxial deformations in graphone as an example. We plot four stress-strain behaviors, which are predicted from the second, third, fourth, and fifth order elastic constants, respectively, compared with the stress-strain curve from DFT calculations (Fig. 3). We find that the linear behaviors predicted from the second order elastic constants are accurate only up to 0.02. Moreover, the third and fourth order elastic constants are accurate up to 0.07 and 0.14, respectively. For an accurate modeling of the stress-

strain behaviors up to its elastic limits, the fifth order elastic constants are indispensable. Similar results are obtained in uniaxial deformations. Such accurately determined strain range is commonly observed in 2D materials^{30–32}. Furthermore, with these elastic constants, any elastic behaviors can be modeled according to elastic theory²⁵.

Like strains, pressure engineering is also a “clean approach to tailor the functions and properties by mechanical load without introducing alien species¹⁸. The Poisson ratio is the ratio between transverse and longitudinal strain, which describes a material's resistance to distortion rather than to change in volume under strains, providing a universal way to contrast the structural performance of a material²⁹. For a general two-dimensional structure, there is a general trend that the Poisson ratio decreases with an increasing in-plane pressure. The mechanism of such a behavior is that the two-dimensional materials are more easily compressed than sheared under a higher pressure. In other words, the normal modes are more sensitive than shear modes. Contrary to this general trend, the Poisson ratio of graphone increases with an increasing in-plane pressure, as shown in Fig. 4, compared to graphene²⁶, graphane²⁶, *h*-BN monolayer²⁵, silicene³³, and MoS₂ monolayers³⁴. Such a behavior was also observed in calculations with different exchange-correlation functionals (Figure S1 in the Supporting Information). This peculiar pressure effect on the Poisson ratio of graphone indicates that the atomic structure of graphone under a higher pressure has a larger tendency to be sheared instead of being compressed. Such a tendency to shear could be an outcome of its atomic structure which has all carbon-hydrogen bonds on one side, lacking the symmetry to balance the shear mode. The reduced symmetry breaks the inversion symmetry. Such an imbalance is a cause of magnetism¹⁵ as well as spin-orbit band splittings⁵.

Interestingly, if we regard a graphane monolayer as two opposite balanced graphone monolayers, we can estimate the value of the Poisson ratio of graphane to be half of that of graphene, which is evidenced by the DFT calculations. Our results suggest a practical way to precisely modulate the structural evolution of nanomaterials under mechanical loads by chemical functionalizations including hydrogenation according to symmetry. Furthermore, we tested the case that all hydrogen atoms of graphane are moved to the same side of carbons, as single-side-hydrogenated graphane³⁵. We found the same trend that the Poisson ratio increases with increasing in-plane pressure in this asymmetric structure, which strongly supports our conclusions.

When the strain increases, the stress increases as shown in Fig. 2, leading to a decrement of pressure. As a consequence, the Poisson ratio decrease, which means that the shear strain decreases, to cause the damping of the strain. As a striking consequence, our finding could lead to a new nanodevice – we named it nano strain damper – to keep unpredictable and

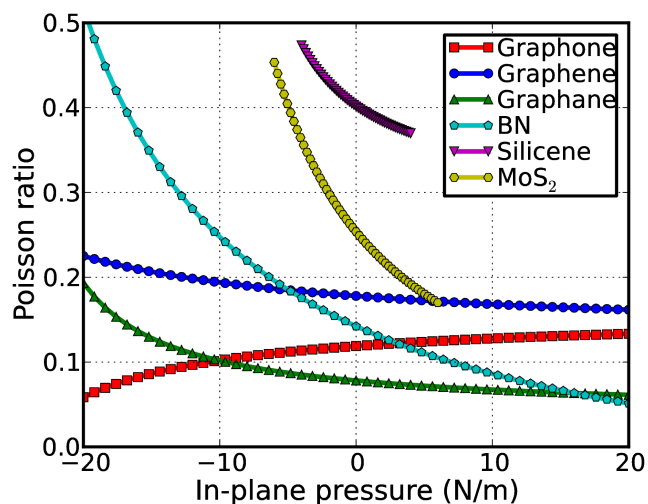


Fig. 4 Pressure effect on the Poisson ratio. The Poisson ratio as a function of the pressure of graphone is peculiar compared to those of other two-dimensional structures including graphene²⁶, graphane²⁶, *h*-BN monolayer²⁵, silicene³³, and MoS₂ monolayers³⁴.

harmful strains away, ensuring the stable performance of a working nanodevice. By precisely controlled hydrogenation, a graphone-like strip can be formed around the target graphene-based devices as a damper to reduce the collateral shear strains from other parts of graphene substrates or all-graphene electronics³⁶.

It is worthy noting that due to limitation of small unit cell and zero temperature, our DFT model can not capture the out-of-plane ripples, which is another important and interesting topic although has little effect on the in-plane stiffness. As temperature rises, the additional thermal stresses will enhance the shear over compression, resulting in larger strain-damping.

The authors would like to acknowledge the generous financial support from the Defense Threat Reduction Agency (DTRA) Grant # BRBAA08-C-2-0130 and # HDTRA1-13-1-0025. Computational resources were provided by Rensselaer Polytechnic Institute through AMOS, the IBM Blue Gene/Q system at the Center for Computational Innovations.

References

- J. Zhou, Q. Wang, Q. Sun, X. S. Chen, Y. Kawazoe and P. Jena, *Nano Lett.*, 2009, **9**, 3867–3870.
- R. Balog, B. Jrgensen, L. Nilsson, M. Andersen, E. Rienks, M. Bianchi, M. Fanetti, E. Lgsgaard, A. Baraldi, S. Lizzit, Z. Sljivancanin, F. Besenbacher, B. Hammer, T. G. Pedersen, P. Hofmann and L. Hornekr, *Nat. Mater.*, 2010, **9**, 315–319.
- D. Haberer, D. V. Vyalikh, S. Taioli, B. Dora, M. Farjam, J. Fink, D. Marchenko, T. Pichler, K. Ziegler, S. Simonucci, M. S. Dresselhaus, M. Knupfer, B. Buchner and A. Gruneis, *Nano Lett.*, 2010, **10**, 3360–3366.
- M. H. Wu, J. D. Burton, E. Y. Tsymbal, X. C. Zeng and P. Jena, *Phys. Rev. B.*, 2013, **87**, 081406.
- M. Gmitra, D. Kochan and J. Fabian, *Phys. Rev. Lett.*, 2013, **110**, 246602.
- S. C. Ray, N. Soin, T. Makgato, C. H. Chuang, W. F. Pong, S. S. Roy, S. K. Ghosh, A. M. Strydom and J. A. McLaughlin, *Sci. Rept.*, 2014, **4**, year.
- Q. Peng, A. K. Dearden, J. Crean, L. Han, S. Liu, X. Wen and S. De, *Nanotechn. Sci. Appl.*, 2014, **7**, 1–29.
- P. Sessi, J. R. Guest, M. Bode and N. P. Guisinger, *Nano Lett.*, 2009, **9**, 4343–4347.
- J. Zhou, M. M. Wu, X. Zhou and Q. Sun, *Appl. Phys. Lett.*, 2009, **95**, 103108.
- J. Zhou and Q. Sun, *Appl. Phys. Lett.*, 2012, **101**, 073114.
- D. C. Elias, R. R. Nair, T. M. G. Mohiuddin, S. V. Morozov, P. Blake, M. P. Halsall, A. C. Ferrari, D. W. Boukhalov, M. I. Katsnelson, A. K. Geim and K. S. Novoselov, *Science*, 2009, **323**, 610–613.
- F. Schwierz, *Nat. Nanotech.*, 2010, **5**, 487–496.
- G. Brumfiel, *Nature*, 2009, **458**, 390–391.
- L. Xie, X. Wang, J. Lu, Z. Ni, Z. Luo, H. Mao, R. Wang, Y. Wang, H. Huang, D. Qi, R. Liu, T. Yu, Z. Shen, T. Wu, H. Peng, B. Ozyilmaz, K. Loh, A. T. S. Wee, Ariando and W. Chen, *Appl. Phys. Lett.*, 2011, **98**, 193113.
- C. D. Reddy, Y. W. Zhang and V. B. Shenoy, *Nanotechnology*, 2012, **23**, 165303.
- N. Kharche and S. K. Nayak, *Nano Lett.*, 2011, **11**, 5274–5278.
- T. Palacios, *Nat. Nanotech.*, 2011, **6**, 464–465.
- F. Guinea, M. I. Katsnelson and A. K. Geim, *Nat. Phys.*, 2010, **6**, 30–33.
- C. Lee, X. Wei, J. W. Kysar and J. Hone, *Science*, 2008, **321**, 385–388.
- A. Zandiatashbar, G.-H. Lee, S. J. An, S. Lee, N. Mathew, M. Terrones, T. Hayashi, C. R. Picu, J. Hone and N. Koratkar, *Nat. Commun.*, 2014, **5**, 3186.
- P. Hohenberg and W. Kohn, *Phys. Rev.*, 1964, **136**, B864.
- G. Kresse and J. Hafner, *Phys. Rev. B*, 1993, **47**, 558.
- R. O. Jones and O. Gunnarsson, *Rev. Mod. Phys.*, 1989, **61**, 689–746.
- J. P. Perdew, K. Burke and M. Ernzerhof, *Phys. Rev. Lett.*, 1996, **77**, 3865–3868.
- Q. Peng, W. Ji and S. De, *Comput. Mater. Sci.*, 2012, **56**, 11 – 17.
- Q. Peng, C. Liang, W. Ji and S. De, *Phys. Chem. Chem. Phys.*, 2013, **15**, 2003–2011.
- M. Topsakal, S. Cahangirov and S. Ciraci, *Appl. Phys. Lett.*, 2010, **96**, 091912.
- Q. Peng, X.-J. Chen, S. Liu and S. De, *RSC Adv.*, 2013, **3**, 7083–7092.
- G. N. Greaves, A. L. Greer, R. S. Lakes and T. Rouxel, *Nat. Mater.*, 2011, **10**, 823–837.
- Q. Peng, X.-J. Chen, W. Ji and S. De, *Adv. Eng. Mater.*, 2013, **15**, 718–727.
- Q. Peng and S. De, *RSC Adv.*, 2013, **3**, 24337 – 24344.
- Q. Peng and S. De, *Nanoscale*, 2014, **6**, 12071–12079.
- Q. Peng, X. Wen and S. De, *RSC Adv.*, 2013, **3**, 13772 – 13781.
- Q. Peng and S. De, *Phys. Chem. Chem. Phys.*, 2013, **15**, 19427 – 19437.
- B. S. Pujari, S. Gusarov, M. Brett and A. Kovalenko, *Phys. Rev. B.*, 2011, **84**, 041402.
- A. K. Geim, *Science*, 2009, **324**, 1530–1534.